Physical Communication 29 (2018) 147–155

Contents lists available at ScienceDirect

Physical Communication

journal homepage: www.elsevier.com/locate/phycom

Full length article

Trellis coded quadrature spatial modulation

Zehra Yigit [a,*], Ertugrul Basar [a], Raed Mesleh [b]

[a] Istanbul Technical University, Faculty of Electrical and Electronics Engineering, 34469, Maslak, Istanbul, Turkey
[b] School of Electrical Engineering and Information Technology, German Jordanian University, Amman-Madaba Street, P.O. Box 35247, Amman 11180, Jordan

ARTICLE INFO

Article history:
Received 28 February 2018
Received in revised form 28 April 2018
Accepted 15 May 2018
Available online 22 May 2018

Keywords:
Spatial modulation
Quadrature spatial modulation
Trellis coded modulation
Nakagami-*m* fading
Rician fading

ABSTRACT

In this paper, a novel multiple-input multiple-output (MIMO) transmission scheme called *trellis coded quadrature spatial modulation* (TC-QSM), is proposed. In the proposed scheme, trellis coded modulation (TCM) principle is applied to the emerging quadrature spatial modulation (QSM) scheme, and a trellis encoder and a QSM mapper are jointly designed to benefit from both coding and multiplexing gains. At the receiver side, a soft-decision Viterbi decoder is used along with a QSM decoder to obtain the optimum error performance. Considering our design criterion, TC-QSM schemes are designed for different number of trellis states, transmit antennas and spectral efficiencies. The pairwise error probability (PEP) of the TC-QSM scheme is derived over quasi-static Nakagami-*m*, Rician and Rayleigh fading channels and an upper bound on the average bit error probability (BEP) is obtained. Through comprehensive Monte Carlo simulations, the effect of signal and spatial bits on uncoded and trellis coded SM and QSM schemes over Nakagami-*m* and Rician fading channels are investigated for different fading parameters. Moreover, the error performance of the TC-QSM and SM with trellis coding (SM-TC) schemes are compared for different spectral efficiency values, where it is revealed that the proposed TC-QSM scheme provides an interesting trade-off between performance and implementation cost, and achieves an improved error performance over reference schemes including SM, QSM and SM-TC.

1. Introduction

Spatial modulation (SM) technique has created a new dimension for multiple-input multiple-output (MIMO) communication technology. In the SM transmission technique, unlike traditional MIMO systems [1], only one of the available transmit antennas is activated and a data symbol selected from M-ary phase shift keying or quadrature amplitude modulation (M-PSK/QAM) constellations is transmitted through this active antenna while the remaining transmit antennas are kept inactive [2]. Since only one transmit antenna is active at any particular time instant in SM, interchannel interference (ICI) is entirely avoided at the receiver side. Its attractive advantages, such as low complexity and high energy efficiency, make SM an alternative to the traditional MIMO systems [3], and this has led researchers to design various SM-based MIMO transmission methods in the past few years. Among many SM-based schemes, two popular forms of SM are space-shift keying (SSK) [4] and generalized SM (GSM) [5]. In the SSK modulation technique, the information is transmitted only through antenna indices. In the GSM scheme, the SM transmission technique is generalized for multiple active antennas in order to improve the spectral efficiency of the classical SM scheme and facilitate the use of arbitrary number of transmit antennas.

SM-based transmission systems enable low-cost and energy-efficient hardware implementation. In [6], for the first time, the bit error rate (BER) performance of the classical SM scheme is experimentally validated. The practical implementation of SSK and GSM schemes are respectively studied in [7] and [8]. The hardware considerations and transmitter designs of different SM-based transmission schemes are proposed in [9].

Quadrature spatial modulation (QSM) is the one of the recently introduced promising MIMO transmission schemes [10]. While, the data symbol is directly transmitted through its related active antenna in SM, a complex M-QAM symbol is separated into its real and imaginary parts in QSM, and these parts are transmitted through their corresponding active antennas, whose indices are independently determined by incoming data bits. Since the real and imaginary parts of a complex M-QAM symbol are conveyed by two orthogonal carriers, ICI is also avoided in the QSM scheme. The QSM technique preserves the inherent advantages of the SM scheme while providing a considerable improvement in the spectral efficiency. Although QSM is a recent MIMO technique, it has attracted substantial attentions in the past two years. Performance of the QSM scheme is analyzed for Nakagami-*m* [11], Rician [12]

* Corresponding author.
E-mail addresses: yigitz@itu.edu.tr (Z. Yigit), basarer@itu.edu.tr (E. Basar), raed.mesleh@gju.edu.jo (R. Mesleh).

https://doi.org/10.1016/j.phycom.2018.05.007
1874-4907/

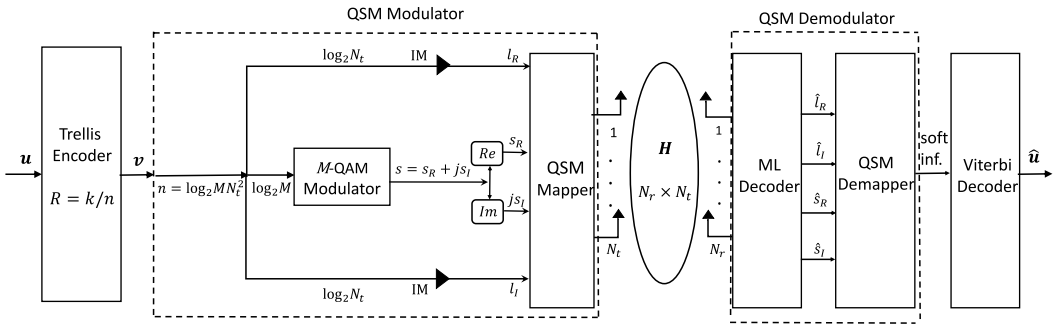

Fig. 1. Block diagram of TC-QSM.

and Weibull [13] fading channels. The error performance of QSM is investigated in the presence of imperfect channel knowledge for Rayleigh [14] and α-μ, κ-μ and η-μ fading channels [15]. In order to reduce the receiver complexity of the QSM based transmission schemes, compressive sensing (CS) [16,17], sphere decoding [18], minimum mean square error (MMSE) [19], equivalent maximum likelihood (ML) [20] and zero forcing (ZF) precoding [21] based low-complexity detectors are designed. In [22,23], the QSM scheme is adopted in traditional cooperative relaying systems and in [24–26], QSM-based cognitive radio (CR) systems are designed to use the spectrum in a more efficient way. In [27], classical QSM scheme is combined with space–time codes to achieve transmit diversity and spatial multiplexing gains at the same time. Furthermore, in [28] and [29], millimeter-wave (mmWave) communications technique, which is a promising transmission technology for next-generation communication systems, is combined with the classical QSM scheme and capacity analysis of the QSM-based mmWave scheme is presented.

Error performance of SM-based systems has been enhanced by a variety of techniques. In [30], the well-known space–time block coding (STBC) principle, the Alamouti's STBC, is combined with the classical SM transmission scheme to simultaneously achieve transmit diversity and spatial multiplexing gains. In [31], polar codes, recently invented by Arikan [32], are integrated to classical SM scheme, and the capacity and the performance results of the system are given. In [33,34], trellis coded modulation (TCM) techniques that are commonly used to improve the error performance without any increase in bandwidth [35], are developed for the SM-MIMO transmission schemes by combining TCM with classical SM in order to simultaneously achieve both coding and multiplexing gains. In [36], the trellis coded SM (TCSM) scheme given in [33] is transformed into a turbo-coded modulation form to further improve the performance of the TCSM scheme. In the SM with trellis coding (SM-TC) scheme [34], after the incoming bits are encoded by a trellis encoder, the coded bits are mapped in accordance with a classical SM mapper, i.e. each branch of the trellis carries a modulated symbol and the index of its corresponding active antenna. At the receiver side of SM-TC, a soft-decision Viterbi decoder is used to process the soft information provided by a SM decoder. The optimum SM-TC schemes are designed for different number of trellis states and spectral efficiency values. In [37], super orthogonal trellis codes (SOTCs) are designed for the classical SM scheme, and finally, the TCM approach is applied to the SSK transmission scheme in [38]. However, the design of trellis coded QSM schemes remains an open and challenging research problem.

In this paper, a novel MIMO transmission technique, which is called *trellis coded quadrature spatial modulation* (TC-QSM), is proposed by combining the aforementioned QSM and TCM schemes. For each transmission interval of the TC-QSM scheme, incoming data bits are encoded by a trellis encoder. The encoded output bits enter a QSM mapper to generate the QSM transmission signals. At the receiver side, a soft-decision Viterbi decoder is utilized to process the soft information provided by an optimum QSM decoder. For different spectral efficiency values, optimum TC-QSM schemes are designed and their corresponding octal generator matrices are given. In addition, theoretical performance analysis of the TC-QSM scheme is performed for Nakagami-m, Rician and Rayleigh fading channels and an upper bound on the average bit error probability (ABEP) is obtained. The considerable bit error rate (BER) improvement of TC-QSM over SM, QSM and SM-TC schemes is demonstrated by computer simulations.

The rest of this paper is organized as follows. The TC-QSM scheme is introduced in Section 2. In Section 3, performance analysis and design criterion of TC-QSM are given. Computer simulation results and our conclusions are presented in Sections 4 and 5, respectively.

2. Trellis coded quadrature spatial modulation

The system model of the TC-QSM scheme operating over a MIMO system configured with N_t transmit and N_r receive antennas is illustrated in Fig. 1. The incoming information bit string $\mathbf{u}$ is encoded by an $R = k/n$ rate trellis encoder and this encoder outputs a bit string of $\mathbf{v}$, which is applied to a QSM modulator. Then, at each transmission period, n coded bits specify the QSM transmit signal, where $n = \log_2(MN_t^2)$ and the overall spectral efficiency is k bits/s/Hz. For the QSM modulator, the first $\log_2(M)$ bits of the incoming n bits determine a complex M-QAM symbol s, which includes both real and imaginary components as $s = s_\Re + js_\Im$ and these components are independently transmitted through the active antennas, whose indices are determined by the remaining $2\log_2(N_t)$ bits. Therefore, the transmit signal generated by the QSM modulator can be represented by $x = (l_\Re, l_\Im, q)$, where $l_\Re$ and $l_\Im$ indicate the active antenna indices corresponding to $s_\Re$ and $js_\Im$, respectively, $l_\Re, l_\Im \in \{1, 2, \ldots, N_t\}$ and q is an element of M-QAM constellation for $q \in \{0, 1, \ldots, M-1\}$. Then, $N_t \times 1$ signal vector

$$\mathbf{x} = \begin{bmatrix} 0 & s_\Re & 0 & \cdots & 0 & js_\Im & 0 \end{bmatrix}^T \tag{1}$$

is transmitted over an $N_r \times N_t$ MIMO channel while experiencing additive white Gaussian noise (AWGN). The channel matrix, which is denoted by $\mathbf{H}$, is assumed to remain unchanged throughout the transmission of a frame, which includes successive transmission periods. Then, the receiver with perfect channel state information (P-CSI) uses a soft-decision Viterbi decoder that utilizes the soft information generated from the QSM decoder to obtain an optimum estimate $\hat{\mathbf{u}}$ for the incoming bit string $\mathbf{u}$.

The main operation concept of the TC-QSM scheme can be presented with an example for $k = 2$ bits/s/Hz and $N_t = 2$. For this TC-QSM scheme, at each transmission period, the trellis encoder with $R = 2/4$ and an octal generator matrix of $\left[\begin{smallmatrix} 2 & 0 & 0 & 1 \\ 0 & 2 & 1 & 0 \end{smallmatrix}\right]$ generates the four-length coded bit string of $\mathbf{v}$, which is processed

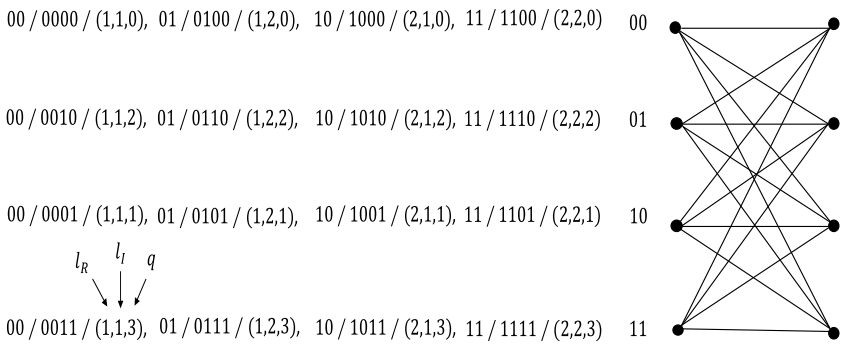

Fig. 2. Trellis diagram of $R = 2/4$ rate TC-QSM with $N_t = 2$ and 4-QAM.

by the QSM encoder as discussed hereinafter. The first and the second coded bits independently determine the active antenna indices corresponding to the real and imaginary parts of a 4-QAM symbol, which is determined by the remaining two bits of $\mathbf{v}$. In Fig. 2, the trellis diagram of this scheme is given, where the state transition of 00/0000/(1, 1, 0) indicates the uncoded input bits $\mathbf{u}$, the coded output bits $\mathbf{v}$ and the QSM symbol of $(l_{\Re}, l_{\Im}, q)$, where $q \in \{0, 1, 2, 3\}$, respectively.

3. Performance analysis and design criterion of the TC-QSM system

In this section, we first derive the conditional pairwise error probability (CPEP) of the TC-QSM scheme and then, use CPEP to obtain the unconditional PEP (UPEP) by considering the channel fading statistics. Assuming that the transmitted codeword $\mathbf{X} = \left[\mathbf{x}^{(1)}, \mathbf{x}^{(2)}, \ldots, \mathbf{x}^{(N)}\right]$ is erroneously detected as $\hat{\mathbf{X}} = \left[\hat{\mathbf{x}}^{(1)}, \hat{\mathbf{x}}^{(2)}, \ldots, \hat{\mathbf{x}}^{(N)}\right]$, where $\mathbf{x}^{(n)}$, $n \in \{1, 2, \ldots, N\}$ is the transmitted QSM vector at the nth transmission interval and N is defined as the length of the corresponding pairwise error event over the trellis. Denoting UPEP of the TC-QSM system and the number of erroneous bits for this error event by $P_r\left(\mathbf{X} \to \hat{\mathbf{X}}\right)$ and $e\left(\mathbf{X}, \hat{\mathbf{X}}\right)$, respectively, the average BEP (ABEP) of the system is upper bounded as

$$P_b \leq \frac{1}{c} \sum_{\mathbf{X}} \left[\frac{1}{k} \sum_{\hat{\mathbf{x}}} P_r\left(\mathbf{X} \to \hat{\mathbf{X}}\right) e\left(\mathbf{X}, \hat{\mathbf{X}}\right) \right] \tag{2}$$

where c is the total number of different error paths of length N. The vector of received signals for the TC-QSM scheme at the nth transmission interval can be given as

$$\begin{aligned} \mathbf{y}^{(n)} &= \mathbf{H}\mathbf{x}^{(n)} + \mathbf{w}^{(n)} \\ &= \mathbf{h}_{l_{\Re}}^{(n)} s_{\Re}^{(n)} + j\mathbf{h}_{l_{\Im}}^{(n)} s_{\Im}^{(n)} + \mathbf{w}^{(n)} \end{aligned} \tag{3}$$

where $\mathbf{w}^{(n)}$ is the $N_r \times 1$ dimensional AWGN samples vector whose elements are independent and identically distributed (i.i.d.) Gaussian random variables with $\mathcal{CN}(0, N_0)$ distribution, and $\mathbf{h}_{l_{\Re}}^{(n)}$ and $\mathbf{h}_{l_{\Im}}^{(n)}$ are the column vectors of the channel matrix $\mathbf{H}$ corresponding to active $l_{\Re}^{(n)}$th and $l_{\Im}^{(n)}$th transmit antennas transmitting $s_{\Re}^{(n)}$ and $js_{\Im}^{(n)}$, respectively. In this paper, we assume that the channel matrix $\mathbf{H}$ is modeled according to (i) Nakagami-m, (ii) Rician and (iii) Rayleigh fading channels.

In case Nakagami-m fading channel is considered, the envelope of each element of $\mathbf{H}$ is distributed according to [39]

$$p(\gamma) = \frac{2m^m \gamma^{2m-1}}{\Gamma(m)} e^{-m\gamma^2} \tag{4}$$

and the elements of $\mathbf{H}$ are modeled as

$$h_l = \sqrt{\sum_{i=1}^{m} |y_i|^2} + j\sqrt{\sum_{i=1}^{m} |z_i|^2} \tag{5}$$

where y_i and z_i are i.i.d. Gaussian random variables with zero mean and $1/2m$ variances.

Rician fading channels consider a dominant line of sight (LoS) component and can be modeled as

$$\mathbf{H} = \sqrt{\frac{K}{K+1}} + \sqrt{\frac{1}{K+1}}\bar{\mathbf{H}} \tag{6}$$

where $\bar{\mathbf{H}}$ is an $N_r \times N_t$ matrix whose entries are i.i.d. complex Gaussian random variables with zero mean and unit-variance, and K is the Rician factor.

Rayleigh distribution is a special case of Nakagami-m distribution for $m = 1$ and Rician distribution for $K = 0$ where $m = \frac{(K+1)^2}{2K+1}$ and each element of the Rayleigh fading channel matrix follows i.i.d. complex Gaussian distribution with zero mean and unit-variance.

Then, for the aforementioned N-length error event, the CPEP of the system is given as

$$\begin{aligned} P_r\left(\mathbf{X} \to \hat{\mathbf{X}}|\mathbf{H}\right) &= P_r\left(\sum_{n=1}^{N} \left\|\mathbf{y}^{(n)} - \mathbf{H}\mathbf{x}^{(n)}\right\|^2 \right. \\ &\left. \geq \sum_{n=1}^{N} \left\|\mathbf{y}^{(n)} - \mathbf{H}\hat{\mathbf{x}}^{(n)}\right\|^2 \middle| \mathbf{H} \right). \end{aligned} \tag{7}$$

After simple manipulations, (7) can be rewritten in the form of

$$\begin{aligned} &P_r\left(\mathbf{X} \to \hat{\mathbf{X}}|\mathbf{H}\right) \\ &= P_r\left(\sum_{n=1}^{N} - \left\|\mathbf{H}\left(\mathbf{x}^{(n)} - \hat{\mathbf{x}}^{(n)}\right)\right\|^2 + 2\Re\left\{\tilde{\mathbf{w}}^{(n)}\right\} \geq 0 \middle| \mathbf{H}\right) \qquad (8) \\ &= P_r\left(D \geq 0 \middle| \mathbf{H}\right) \qquad (9) \end{aligned}$$

where $\tilde{\mathbf{w}}^{(n)} = (\mathbf{w}^{(n)})^H\left(\mathbf{H}\left(\mathbf{x}^{(n)} - \hat{\mathbf{x}}^{(n)}\right)\right)$ and D is a Gaussian random variable which is called decision variable compared with a zero threshold [40], and it is distributed as $\mathcal{CN}(m_D, \sigma_D^2)$ with $m_D = -\sum_{n=1}^{N}\left\|\mathbf{H}\left(\mathbf{x}^{(n)} - \hat{\mathbf{x}}^{(n)}\right)\right\|^2$ and $\sigma_D^2 = 2N_0\sum_{n=1}^{N}\left\|\mathbf{H}\left(\mathbf{x}^{(n)} - \hat{\mathbf{x}}^{(n)}\right)\right\|^2$. Finally, the CPEP can be expressed in terms of the Q-function as

$$P_r\left(\mathbf{X} \to \hat{\mathbf{X}}|\mathbf{H}\right) = Q\left(\frac{-m_D}{\sigma_D}\right) = Q\left(\sqrt{\frac{\Lambda}{2N_0}}\right). \tag{10}$$

Here, Λ can be given as the following, for $\mathbf{S}_n = \left(\mathbf{x}^{(n)} - \hat{\mathbf{x}}^{(n)}\right)^H \left(\mathbf{x}^{(n)} - \hat{\mathbf{x}}^{(n)}\right)$:

$$\begin{aligned}\Lambda &= \sum_{n=1}^{N} \left\| \mathbf{H}\left(\mathbf{x}^{(n)} - \hat{\mathbf{x}}^{(n)}\right)\right\|^2 \\ &= \mathrm{Tr}\left(\sum_{n=1}^{N} \mathbf{H}^H \left(\mathbf{x}^{(n)} - \hat{\mathbf{x}}^{(n)}\right)^H \left(\mathbf{x}^{(n)} - \hat{\mathbf{x}}^{(n)}\right)\mathbf{H}\right) \\ &= \mathrm{vec}(\mathbf{H}^H)^H (\mathbf{I}_{N_r} \otimes \mathbf{S}) \mathrm{vec}(\mathbf{H}^H)\end{aligned} \tag{11}$$

where $\mathbf{S} = \sum_{n=1}^{N} \mathbf{S}_n$, $\mathrm{Tr}(\cdot)$ represents the trace of a matrix, $\mathrm{vec}(\cdot)$ is the vectorization operator, $\otimes$ denotes the Kronecker product, and $\mathbf{I}_{N_r}$ is $N_r \times N_r$ identity matrix.

Using $Q(x) = \frac{1}{\pi}\int_0^{\pi/2} \exp\left(-\frac{x^2}{2\sin^2\theta}\right) d\theta$ and substituting (11) into this alternative expression, (10) yields

$$P_r\left(\mathbf{X} \to \hat{\mathbf{X}}|\mathbf{H}\right) = \frac{1}{\pi}\int_0^{\pi} \exp\left(-\varphi \frac{\mathrm{vec}(\mathbf{H}^H)^H \boldsymbol{\Delta} \mathrm{vec}(\mathbf{H}^H)}{4\sin^2\theta}\right) d\theta \tag{12}$$

where $\varphi = 1/N_0$ and $\boldsymbol{\Delta} = \mathbf{I}_{N_r} \otimes \mathbf{S}$. After that, the PEP of the system is expressed considering the moment generating function (MGF) approach as follows

$$P_r\left(\mathbf{X} \to \hat{\mathbf{X}}\right) = \frac{1}{\pi}\int_0^{\pi/2} \mathcal{M}_{\Lambda}\left(-\frac{\varphi}{4\sin^2\theta}\right) d\theta. \tag{13}$$

To evaluate the MGF in (13), we use the MGF of the quadratic form $\mathbf{z}^H\mathbf{B}\mathbf{z}$ [41], which is given as

$$\mathcal{M}(s) = \frac{\exp[s\bar{\mathbf{z}}^H \mathbf{B}(\mathbf{I} - s\mathbf{C}_{\mathbf{z}}\mathbf{B})^{-1}\bar{\mathbf{z}}]}{\det(\mathbf{I} - s\mathbf{C}_{\mathbf{z}}\mathbf{B})} \tag{14}$$

where $\mathbf{B}$ is a Hermitian matrix and $\mathbf{z}$ is a circularly symmetric Gaussian vector with mean vector of $\bar{\mathbf{z}}$ and the covariance matrix $\mathbf{C}_{\mathbf{z}} = E\left\{\mathbf{z}^H\mathbf{z}\right\} - \bar{\mathbf{z}}^H\bar{\mathbf{z}}$. Letting $\mathbf{z} = \mathrm{vec}(\mathbf{H}^H)$ and $\mathbf{B} = \boldsymbol{\Delta}$, the PEP of the TC-QSM scheme is evaluated as

$$P_r\left(\mathbf{X} \to \hat{\mathbf{X}}\right) = \frac{1}{\pi}\int_0^{\pi/2} \frac{\exp\left(-\bar{\mathbf{z}}^H \frac{\varphi}{4\sin^2\theta}\boldsymbol{\Delta}\left(\mathbf{I}_{N_tN_r} + \frac{\varphi}{4\sin^2\theta}\mathbf{C}_{\mathbf{z}}\boldsymbol{\Delta}\right)^{-1}\bar{\mathbf{z}}\right)}{\det\left(\mathbf{I}_{N_tN_r} + \frac{\varphi}{4\sin^2\theta}\mathbf{C}_{\mathbf{z}}\boldsymbol{\Delta}\right)} d\theta. \tag{15}$$

When Nakagami-m fading channel is considered, the mean vector $\bar{\mathbf{z}}$ and the covariance matrix $\mathbf{C}_{\mathbf{z}}$ are given respectively as [14]

$$\begin{aligned}\bar{\mathbf{z}} &= \left(\frac{\Gamma((\frac{m}{2}) + \frac{1}{2})}{\Gamma(\frac{m}{2})\sqrt{\frac{m}{2}}} e^{j\frac{\pi}{4}}\right) \times \mathrm{vec}(\mathbf{1}_{NtNr}) \\ \mathbf{C}_{\mathbf{z}} &= \left(1 - \frac{2}{m}\left(\frac{\Gamma((\frac{m}{2}) + \frac{1}{2})}{\Gamma(\frac{m}{2})}\right)^2\right) \times \mathbf{I}_{N_tN_r}\end{aligned} \tag{16}$$

where $\mathbf{1}_{NtNr}$ and $\mathbf{I}_{N_tN_r}$ are $N_tN_r \times N_tN_r$ dimensional all-ones and identity matrices, respectively. Then, the PEP of the system is founded by substituting (16) into (15).

For the case of Rician fading channel, $\bar{\mathbf{z}}$ and $\mathbf{C}_{\mathbf{z}}$ become

$$\begin{aligned}\bar{\mathbf{z}} &= \sqrt{\frac{K}{K+1}} \times \mathrm{vec}(\mathbf{1}_{NtNr}) \\ \mathbf{C}_{\mathbf{z}} &= \frac{1}{1+K} \times \mathbf{I}_{N_tN_r}.\end{aligned} \tag{17}$$

Therefore, the PEP of the TC-QSM system over Rician fading channel can be calculated from

$$P_r\left(\mathbf{X} \to \hat{\mathbf{X}}\right) = \frac{1}{\pi}\int_0^{\pi/2} \frac{\exp\left(-\bar{\mathbf{z}}^H \frac{\varphi}{4\sin^2\theta}\boldsymbol{\Delta}\left(\mathbf{I}_{N_tN_r} + \frac{\varphi}{4(K+1)\sin^2\theta}\boldsymbol{\Delta}\right)^{-1}\bar{\mathbf{z}}\right)}{\det\left(\mathbf{I}_{N_tN_r} + \frac{\varphi}{4(K+1)\sin^2\theta}\boldsymbol{\Delta}\right)} d\theta. \tag{18}$$

The exact result of the integral in (15) can be easily evaluated by using computer software. Nevertheless, to derive a closed form expression, we obtain an upper bound by letting $\theta = \frac{\pi}{2}$ in (15) yielding

$$P_r\left(\mathbf{X} \to \hat{\mathbf{X}}\right) \le \frac{1}{2}\frac{\exp\left(-\bar{\mathbf{z}}^H \frac{\varphi}{4}\boldsymbol{\Delta}\left(\mathbf{I}_{N_tN_r} + \frac{\varphi}{4}\mathbf{C}_{\mathbf{z}}\boldsymbol{\Delta}\right)^{-1}\bar{\mathbf{z}}\right)}{\det\left(\mathbf{I}_{N_tN_r} + \frac{\varphi}{4}\mathbf{C}_{\mathbf{z}}\boldsymbol{\Delta}\right)}. \tag{19}$$

Therefore, the PEP of the system over Rician fading channels can be upper bounded as

$$P_r\left(\mathbf{X} \to \hat{\mathbf{X}}\right) \le \frac{1}{2}\frac{\exp\left(-\bar{\mathbf{z}}^H \frac{\varphi}{4}\boldsymbol{\Delta}\left(\mathbf{I}_{N_tN_r} + \frac{\varphi}{4(K+1)}\boldsymbol{\Delta}\right)^{-1}\bar{\mathbf{z}}\right)}{\det\left(\mathbf{I}_{N_tN_r} + \frac{\varphi}{4(K+1)}\boldsymbol{\Delta}\right)}. \tag{20}$$

When Rayleigh fading channel, which is the special case of Nakagami-m and Rician fading channels, respectively, for $m = 1$ and $K = 0$, is assumed, the PEP upper bound of the system can be simply given as

$$P_r\left(\mathbf{X} \to \hat{\mathbf{X}}\right) \le \frac{1}{2}\left[\det\left(\mathbf{I}_{N_t} + \frac{\varphi}{4}\mathbf{S}\right)\right]^{-Nr} \tag{21}$$

where $\mathbf{I}_{N_t}$ is $N_t \times N_t$ identity matrix.

3.1. Design criterion of the TC-QSM system

The UPEP derivation of (19) clearly shows that the error performance of the TC-QSM system directly depends on the characteristics of the $\mathbf{S}$ matrix. Using rank additivity [42], we have $\mathrm{rank}(\mathbf{S}) \le \sum_{n=1}^{N} \mathrm{rank}(\mathbf{S}_n)$ for $\sum_{n=1}^{N} \mathrm{rank}(\mathbf{S}_n) \ge N$, since $\mathrm{rank}(\mathbf{S}_n) \ge 1$ depending on the number of transmit antennas N_t and the fading coefficients of $\mathbf{h}_{\Re}^{(n)}$ and $\mathbf{h}_{\Im}^{(n)}$. $\mathbf{S}_n$ is formed by considering channel coefficients of $\mathbf{h}_{l_{\Re}}^{(n)}$, $\mathbf{h}_{l_{\Im}}^{(n)}$, $\hat{\mathbf{h}}_{\hat{l}_{\Re}}^{(n)}$ and $\hat{\mathbf{h}}_{\hat{l}_{\Im}}^{(n)}$ for the corresponding selected antenna indices of $l_{\Re}^{(n)}$ and $l_{\Im}^{(n)}$ and detected antenna indices of $\hat{l}_{\Re}^{(n)}$ and $\hat{l}_{\Im}^{(n)}$, where the entries of $\mathbf{S}_n$ can be formed by considering summation of $\mathbf{S}_n = \sum_{i=1}^{6} \mathbf{S}_n^i$ for the following cases:

– if $l_{\Re}^{(n)} = l_{\Im}^{(n)}$

$$\mathbf{S}_n^1(p,q) = \begin{cases} \left|s_{\Re}^{(n)} + js_{\Im}^{(n)}\right|^2 & \text{if } p = q = l_{\Re}^{(n)} \\ 0 & \text{otherwise} \end{cases}$$

or $l_{\Re}^{(n)} \neq l_{\Im}^{(n)}$

$$\mathbf{S}_n^1(p,q) = \begin{cases} \left|s_{\Re}^{(n)}\right|^2 & \text{if } p = q = l_{\Re}^{(n)} \\ \left|s_{\Im}^{(n)}\right|^2 & \text{if } p = q = l_{\Im}^{(n)} \\ js_{\Im}^{(n)} s_{\Re}^{(n)} & \text{if } p = l_{\Re}^{(n)}, q = l_{\Im}^{(n)} \\ -js_{\Im}^{(n)} s_{\Re}^{(n)} & \text{if } p = l_{\Im}^{(n)}, q = l_{\Re}^{(n)} \end{cases} \tag{22}$$

– if $\hat{l}_{\Re}^{(n)} = \hat{l}_{\Im}^{(n)}$

$$\mathbf{S}_n^2(p,q) = \begin{cases} \left|\hat{s}_{\Re}^{(n)} + j\hat{s}_{\Im}^{(n)}\right|^2 & \text{if } p = q = \hat{l}_{\Re}^{(n)} \\ 0 & \text{otherwise} \end{cases}$$

or $\hat{l}_{\Re}^{(n)} \neq \hat{l}_{\Im}^{(n)}$

$$\mathbf{S}_n^2(p,q) = \begin{cases} \left|\hat{s}_{\Re}^{(n)}\right|^2 & \text{if } p = q = \hat{l}_{\Re}^{(n)} \\ \left|\hat{s}_{\Im}^{(n)}\right|^2 & \text{if } p = q = \hat{l}_{\Im}^{(n)} \\ j\hat{s}_{\Im}^{(n)} \hat{s}_{\Re}^{(n)} & \text{if } p = \hat{l}_{\Re}^{(n)}, q = \hat{l}_{\Im}^{(n)} \\ -j\hat{s}_{\Im}^{(n)} \hat{s}_{\Re}^{(n)} & \text{if } p = \hat{l}_{\Im}^{(n)}, q = \hat{l}_{\Re}^{(n)} \end{cases} \tag{23}$$

– if $l_{\Re}^{(n)} = \hat{l}_{\Re}^{(n)}$

$$\mathbf{S}_n^3(p,q) = \begin{cases} -2s_{\Re}^{(n)}\hat{s}_{\Re}^{(n)} & p = q = l_{\Re}^{(n)} \\ 0 & \text{otherwise} \end{cases}$$

or $l_{\Re}^{(n)} \neq \hat{l}_{\Re}^{(n)}$

$$\mathbf{S}_n^3(p,q) = \begin{cases} -s_{\Re}^{(n)}\hat{s}_{\Re}^{(n)} & p = l_{\Re}^{(n)}, q = \hat{l}_{\Re}^{(n)} \\ -s_{\Re}^{(n)}\hat{s}_{\Re}^{(n)} & p = \hat{l}_{\Re}^{(n)}, q = l_{\Re}^{(n)} \end{cases} \tag{24}$$

– if $l_{\Re}^{(n)} \neq \hat{l}_{\Im}^{(n)}$

$$\mathbf{S}_n^4(p,q) = \begin{cases} -j\hat{s}_{\Im}^{(n)}s_{\Re}^{(n)} & p = l_{\Re}^{(n)}, q = \hat{l}_{\Im}^{(n)} \\ j\hat{s}_{\Im}^{(n)}s_{\Re}^{(n)} & p = \hat{l}_{\Im}^{(n)}, q = l_{\Re}^{(n)} \end{cases} \tag{25}$$

or $l_{\Re}^{(n)} = \hat{l}_{\Im}^{(n)}$

$$\mathbf{S}_n^4(p,q) = 0 \qquad \text{for all } p \text{ and } q$$

– if $l_{\Im}^{(n)} = \hat{l}_{\Im}^{(n)}$

$$\mathbf{S}_n^5(p,q) = \begin{cases} -2s_{\Im}^{(n)}\hat{s}_{\Im}^{(n)} & p = q = l_{\Im}^{(n)} \\ 0 & \text{otherwise} \end{cases}$$

or $l_{\Im}^{(n)} \neq \hat{l}_{\Im}^{(n)}$

$$\mathbf{S}_n^5(p,q) = \begin{cases} -s_{\Im}^{(n)}\hat{s}_{\Im}^{(n)} & p = l_{\Im}^{(n)}, q = \hat{l}_{\Im}^{(n)} \\ -s_{\Im}^{(n)}\hat{s}_{\Im}^{(n)} & p = \hat{l}_{\Im}^{(n)}, q = l_{\Im}^{(n)} \end{cases} \tag{26}$$

– if $l_{\Im}^{(n)} \neq \hat{l}_{\Re}^{(n)}$

$$\mathbf{S}_n^6(p,q) = \begin{cases} -j\hat{s}_{\Re}^{(n)}s_{\Im}^{(n)} & p = l_{\Im}^{(n)}, q = \hat{l}_{\Re}^{(n)} \\ j\hat{s}_{\Re}^{(n)}s_{\Im}^{(n)} & p = \hat{l}_{\Re}^{(n)}, q = l_{\Im}^{(n)} \end{cases} \tag{27}$$

or $l_{\Im}^{(n)} = \hat{l}_{\Re}^{(n)}$

$$\mathbf{S}_n^6(p,q) = 0 \qquad \text{for all } p \text{ and } q.$$

In the following, we provide an example for the formation of $\mathbf{S}_n$.

Example. For the case of $N_t = 4$ and $N_r = 1$ with $h_{\Re}^{(n)} = h_1$, $h_{\Im}^{(n)} = h_4$, $\hat{h}_{\Re}^{(n)} = h_2$ and $\hat{h}_{\Im}^{(n)} = h_3$ (i.e, $l_{\Re}^{(n)} = 1$, $l_{\Im}^{(n)} = 4$, $\hat{l}_{\Re}^{(n)} = 2$ and $\hat{l}_{\Im}^{(n)} = 3$), $\mathbf{S}_n$ is obtained as

$$\mathbf{S}_n = \begin{bmatrix} |s_{\Re}^{(n)}|^2 & -s_{\Re}^{(n)}\hat{s}_{\Re}^{(n)} & -js_{\Re}^{(n)}\hat{s}_{\Im}^{(n)} & js_{\Re}^{(n)}s_{\Im}^{(n)} \\ -\hat{s}_{\Re}^{(n)}s_{\Re}^{(n)} & |\hat{s}_{\Re}^{(n)}|^2 & j\hat{s}_{\Re}^{(n)}\hat{s}_{\Im}^{(n)} & -j\hat{s}_{\Re}^{(n)}s_{\Im}^{(n)} \\ j\hat{s}_{\Im}^{(n)}s_{\Re}^{(n)} & -j\hat{s}_{\Im}^{(n)}\hat{s}_{\Re}^{(n)} & |\hat{s}_{\Im}^{(n)}|^2 & -\hat{s}_{\Im}^{(n)}s_{\Im}^{(n)} \\ -js_{\Im}^{(n)}s_{\Re}^{(n)} & js_{\Im}^{(n)}\hat{s}_{\Re}^{(n)} & -s_{\Im}^{(n)}\hat{s}_{\Im}^{(n)} & |s_{\Im}^{(n)}|^2 \end{bmatrix}. \tag{28}$$

The degrees of freedom (DOF) for the TC-QSM system is the number of rows or columns of $\mathbf{S}$ without all zero elements, which is equivalent to the overall number of different channel realizations. Therefore, the necessary condition for an N-length error event to achieve Nth order diversity is DOF $\geq N$ [34]. Considering this design criterion, we provide a number of TC-QSM schemes for $k = 2$, 3 and 4 bits/s/Hz, where the generator matrix of each design ($\mathbf{G}_{k/n}$) is given in Table 1. The $R = 2/4$ TC-QSM scheme with a generator matrix of $\mathbf{G}_{2/4}$ is configured for $N_t = 2$ and 4-QAM ensuring DOF $= 2$ for $N = 2$ at 2 bits/s/Hz. The 2/6-rate TC-QSM scheme with a generator matrix of $\mathbf{G}_{2/6}$ uses $N_t = 4$ and 4-QAM, and guarantees DOF ≥ 3 for $N = 3$ at 2 bits/s/Hz. Similarly, for the TC-QSM schemes with 3/6 and 4/8 rates, generator matrices of $\mathbf{G}_{3/6}$ and $\mathbf{G}_{4/8}$ are constructed, respectively, considering 4-QAM constellation with $N_t = 4$ and $N_t = 8$, and both designs ensure DOF ≥ 3 for $N = 2$.

4. Simulation results

In this section, the BER performance of the SM-TC and TC-QSM schemes is analyzed over Nakagami-m and Rician fading channels for different m and K values, respectively. Then, theoretical ABEP performance of the SM-TC and TC-QSM system is derived over Nakagami-m, Rician and Rayleigh fading channels and an upper bound is obtained, which is corroborated via Monte Carlo simulations for different MIMO configurations and number of trellis states. The BER performance of TC-QSM schemes is provided for 2, 3 and 4 bits/s/Hz spectral efficiencies while considering the average signal to noise ratio (SNR) per each receive antenna. Moreover, the BER performance of the TC-QSM scheme is compared with SM-TC, SM and QSM schemes. For all cases, the simulations are performed for $N_r = 2$ and the channel fading coefficients are assumed to remain unchanged for a frame duration, where a frame is consisted of 20 successive transmissions.

Table 1
Generator matrices of TC-QSM schemes with different coding rates.

k [bits/s/Hz]	# of states	Generator matrix
2	4	$\mathbf{G}_{2/4} = \begin{bmatrix} 2 & 0 & 0 & 1 \\ 0 & 2 & 1 & 0 \end{bmatrix}$
2	16	$\mathbf{G}_{2/6} = \begin{bmatrix} 6 & 2 & 1 & 3 & 1 & 0 \\ 1 & 5 & 3 & 2 & 0 & 1 \end{bmatrix}$
3	8	$\mathbf{G}_{3/6} = \begin{bmatrix} 1 & 1 & 2 & 2 & 2 & 0 \\ 1 & 2 & 1 & 0 & 0 & 2 \\ 1 & 0 & 0 & 1 & 0 & 0 \end{bmatrix}$
4	16	$\mathbf{G}_{4/8} = \begin{bmatrix} 1 & 1 & 3 & 1 & 0 & 0 & 0 & 1 \\ 1 & 0 & 0 & 0 & 1 & 0 & 0 & 0 \\ 0 & 1 & 1 & 1 & 0 & 1 & 0 & 0 \\ 0 & 3 & 1 & 0 & 1 & 2 & 1 & 0 \end{bmatrix}$

To observe the effect of increasing Nakagami-m values on the overall BER performance of SM-based schemes, the signal bit error rate (BER1) and spatial bit error rate (BER2) of classical SM and QSM schemes are given for $m = 2$ and $m = 4$, in Figs. 3(a) and 3(b), respectively. It is clearly seen from these figures that for both uncoded SM and QSM schemes, increasing m values improve BER1 while degrade BER2, where SM uses $N_t = 4$ with QPSK and QSM uses $N_t = 2$ with 4-QAM. We conclude that the poor BER2 performance causes degradation in the overall BER performance of both uncoded SM and QSM schemes.

In Fig. 4, for 2 bits/s/Hz, the performance of the signal BER (BER1) and spatial BER (BER2) curves of SM-TC and TC-QSM schemes are depicted over Nakagami-m fading channels for $m = 2$ and $m = 4$. For this case, BER1 and BER2 respectively indicate the error probability for the signal and spatial bits of the coded bit sequence of $\mathbf{v}$. In Figs. 4(a) and 4(b), BER1, BER2 and the overall BER performance of the 2/4-rate SM-TC and 2/4-rate TC-QSM schemes are given, respectively, where the 2/4-rate SM-TC scheme with 4 states uses $N_t = 4$ and QPSK, and the 2/4-rate TC-QSM scheme with 4 states uses $N_t = 2$ and 4-QAM. It is observed that contrary to the uncoded SM and QSM schemes, the trellis coded SM-based systems enhance the overall BER performance as m increases. This phenomenon can be explained by the fact that compared to uncoded SM and QSM schemes, the trellis coding structure significantly enhances the performance of BER2 so that the overall BER performance of SM-TC and TC-QSM improves and almost corresponds to BER1. Moreover, in both figures, we observe that the theoretical results of the SM-TC and TC-QSM schemes are consistent with the Monte Carlo simulations which validate the accuracy of the derived formulas.

In Figs. 5(a) and 5(b), for 2 bits/s/Hz, the effects of signal and spatial bit errors on the overall error performance of the SM-TC and the TC-QSM schemes over Rician fading channels for the Rician factors of $K = 2$ and $K = 7$ are carried out. Similar to the performance over Nakagami-m channels, both SM-TC and TC-QSM schemes achieve an improvement in the overall BER performance with increasing K values, where in Fig. 5(a), 2/4-rate SM-TC with

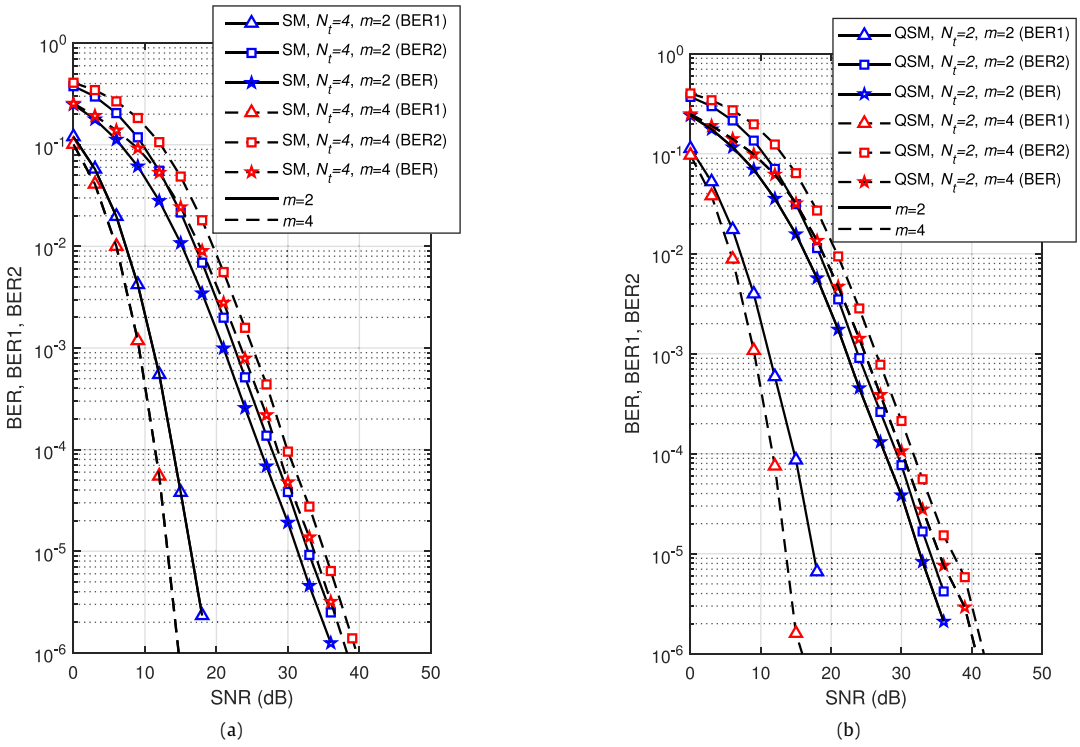

Fig. 3. Performance of signal BER (BER1) and spatial BER (BER2) of the uncoded (a) SM and (b) QSM systems over Nakagami-m channels for $m = 2$ and $m = 4$.

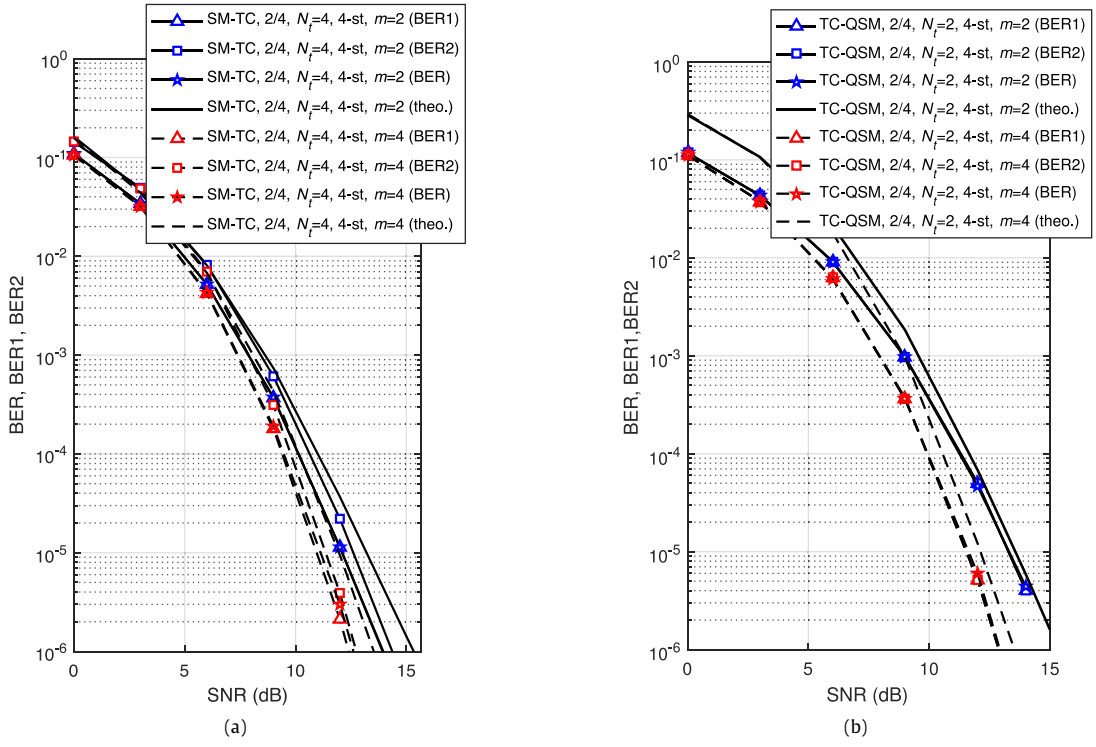

Fig. 4. Performance of signal BER (BER1) and spatial BER (BER2) of the (a) SM-TC and (b) TC-QSM systems over Nakagami-m channels for $m = 2$ and $m = 4$.

4 states uses $N_t = 4$ and QPSK while in Fig. 5(b), 2/6-rate TC-QSM with 16 states uses $N_t = 4$ and 4-QAM. The theoretical results supporting the Monte Carlo simulation results of the SM-TC and the TC-QSM schemes over Rician fading channels are also illustrated. In Figs. 4(a) and 5(a), the simulation results of the SM-TC scheme over Nakagami-m and Rician fading channels move away from the ABEP curves after a particular signal to noise (SNR) value, where similar behaviors were encountered in SM-TC [34]

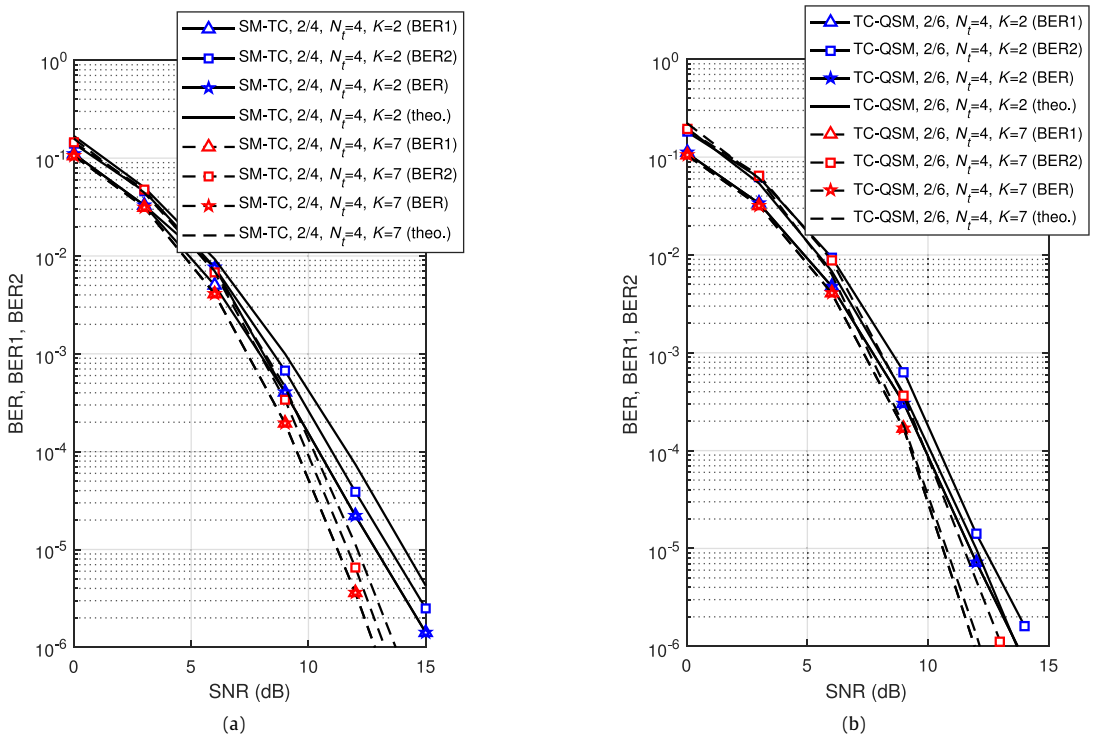

Fig. 5. Performance of signal BER (BER1) and spatial BER (BER2) of the (a) SM-TC and (b) TC-QSM systems over Rician fading channels for $K = 2$ and $K = 7$.

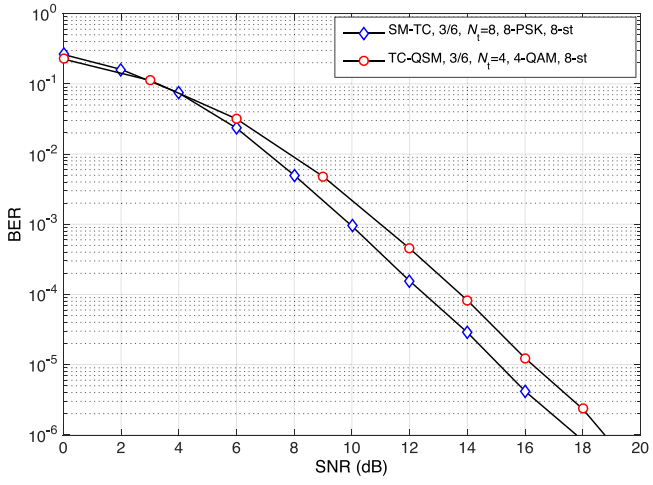

Fig. 6. Performance comparison of the 8-state TC-QSM and SM-TC schemes at 3 bits/s/Hz over Rayleigh fading channels.

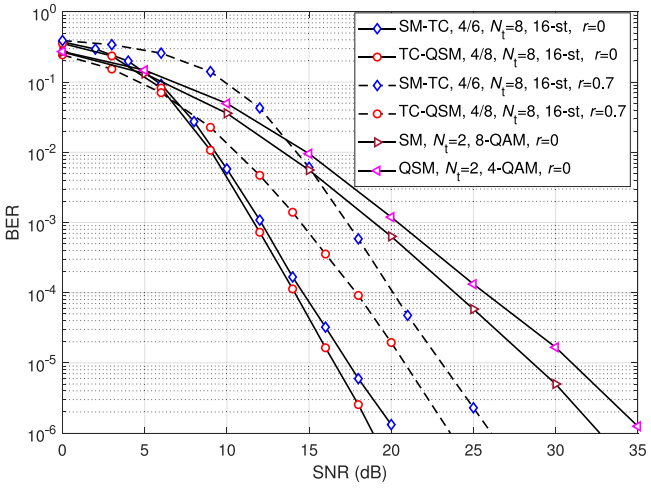

Fig. 7. Performance comparison of 16-state SM-TC and TC-QSM schemes at 4 bits/s/Hz over correlated ($r = 0.7$) and uncorrelated ($r = 0$) Rayleigh fading channels.

and trellis coded SSK [38] over Rayleigh fading channels. It is worth noting that this mismatch is caused by the nature of the considered union bound for trellis coded schemes.

In Fig. 6, for 3 bits/s/Hz spectral efficiency, the error performance of TC-QSM is compared with the SM-TC scheme over Rayleigh fading channels ($m = 1$ or $K = 0$). For the 8 states SM-TC scheme, $N_t = 8$ with 8-PSK is used. However, TC-QSM scheme achieves 3 bits/s/Hz using $N_t = 4$ with 4-QAM. Depicted results reveal that SM-TC exhibits 1 dB SNR gain compared to TC-QSM scheme. The improved BER performance of the SM-TC scheme over the TC-QSM can be explained by the fact that for 8 states and 3 bits/s/Hz spectral efficiency, the number of transmit antennas used by TC-QSM is half that of the SM-TC scheme. Therefore, the SM-TC scheme with larger MIMO antenna configuration provides a better error performance than the TC-QSM scheme, which exhibits an interesting trade-off between the BER performance and the implementation cost.

In Fig. 7, the BER performance of the TC-QSM and the SM-TC schemes are given for 4 bits/s/Hz over Rayleigh fading channels in the presence of correlated and uncorrelated fading conditions. The 4/8-rate TC-QSM scheme with 16 states uses $N_t = 8$ and 4-QAM, while the 4/6 SM-TC with 16 states uses $N_t = 8$ with 8-PSK. For this case, both TC-QSM and SM-TC achieve 4 bits/s/Hz spectral efficiency with identical number of transmit antennas, where $N_t = 8$. In this figure, the effect of spatial correlation (SC)

is analyzed by modeling correlated channel matrix $\mathbf{H}_{SC}$ using the Kronecker model [43] as

$$\mathbf{H}_{SC} = \mathbf{R}_r^{1/2}\mathbf{H}\mathbf{R}_t^{1/2} \tag{29}$$

where $\mathbf{R}_r \in \mathbb{C}^{N_r \times N_r}$ and $\mathbf{R}_t \in \mathbb{C}^{N_t \times N_t}$ are the receiver and transmitter correlation matrices, respectively. For the correlation coefficient of r, $\mathbf{R}_r$ and $\mathbf{R}_t$ are given as

$$\mathbf{R}_r = \begin{bmatrix} 1 & r & r^2 & \cdots & r^{N_r-1} \\ r & 1 & r & \cdots & r^{N_r-2} \\ r^2 & r & 1 & \cdots & r^{N_r-3} \\ \vdots & \vdots & \vdots & \ddots & \vdots \\ r^{N_r-1} & r^{N_r-2} & r^{N_r-3} & \cdots & 1 \end{bmatrix},$$

$$\mathbf{R}_t = \begin{bmatrix} 1 & r & r^2 & \cdots & r^{N_t-1} \\ r & 1 & r & \cdots & r^{N_t-2} \\ r^2 & r & 1 & \cdots & r^{N_t-3} \\ \vdots & \vdots & \vdots & \ddots & \vdots \\ r^{N_t-1} & r^{N_t-2} & r^{N_t-3} & \cdots & 1 \end{bmatrix}. \tag{30}$$

The simulation results indicate that for uncorrelated fading conditions, $r = 0$, TC-QSM scheme exhibits a 1 dB SNR gain over SM-TC at a target BER value of 10^{-6}, while for $r = 0.7$, the SNR gain of TC-QSM over SM-TC reaches 3 dB at the BER value of 10^{-6}. It can be also clearly observed from Fig. 7 that despite high correlation, TC-QSM and SM-TC schemes still provide significantly better BER performance over uncoded QSM and SM schemes.

5. Conclusion

In this paper, a novel coded MIMO transmission scheme combining TCM and QSM, is proposed to benefit from the advantages of both techniques. The proposed TC-QSM scheme has been theoretically analyzed over Nakagami-m, Rician and Rayleigh fading channels and an expression for the UPEP of the TC-QSM has been derived. Then, theoretical upper bounds for the ABEP performance are obtained. Furthermore, the effects of the signal and spatial errors of the SM, QSM [14], SM-TC [34] and TC-QSM schemes have been investigated. Reported results have revealed that contrary to uncoded SM and QSM schemes, trellis coded versions of the SM-TC and the TC-QSM improve the overall BER performance with increasing m and K values by improving the performance of spatial bits compared to uncoded SM and QSM schemes. Moreover, the error performance of TC-QSM has been compared with the reference SM-TC structure for different spectral efficiency values and it has been shown that when the same number of transmit antennas is considered, the TC-QSM scheme outperforms the reference SM-TC scheme.

References

[1] G.J. Foschini, Layered space-time architecture for wireless communication in a fading environment when using multi-element antennas, Bell Labs Tech. J. 1 (2) (1996) 41–59. http://dx.doi.org/10.1002/bltj.2015.

[2] R.Y. Mesleh, H. Haas, S. Sinanovic, C.W. Ahn, S. Yun, Spatial modulation, IEEE Trans. Veh. Technol. 57 (4) (2008) 2228–2241. http://dx.doi.org/10.1109/TVT.2007.912136.

[3] E. Basar, Index modulation techniques for 5G wireless networks, IEEE Commun. Mag. 54 (7) (2016) 168–175. http://dx.doi.org/10.1109/MCOM.2016.7509396.

[4] J. Jeganathan, A. Ghrayeb, L. Szczecinski, A. Ceron, Space shift keying modulation for MIMO channels, IEEE Trans. Wireless Commun. 8 (7) (2009) 3692–3703. http://dx.doi.org/10.1109/TWC.2009.080910.

[5] A. Younis, N. Serafimovski, R. Mesleh, H. Haas, Generalised spatial modulation, in: Proc. Signals, Systems and Computers (ASILOMAR), 2010. http://dx.doi.org/10.1109/ACSSC.2010.5757786.

[6] N. Serafimovski, A. Younis, R. Mesleh, P. Chambers, M. Di Renzo, C.-X. Wang, P.M. Grant, M.A. Beach, H. Haas, Practical implementation of spatial modulation, IEEE Trans. Veh. Technol. 62 (9) (2013) 4511–4523. http://dx.doi.org/10.1109/TVT.2013.2266619.

[7] A. Afana, S. Ikki, Analytical framework for space shift keying MIMO systems with hardware impairments and co-channel interference, IEEE Commun. Lett. 21 (3) (2017) 488–491. http://dx.doi.org/10.1109/LCOMM.2016.2634014.

[8] R. Mesleh, O. Hiari, A. Younis, Generalized space modulation techniques: Hardware design and considerations, Phys. Commun. 26 (2018) 87–95. http://dx.doi.org/10.1016/j.phycom.2017.11.009.

[9] R. Mesleh, O. Hiari, A. Younis, S. Alouneh, Transmitter design and hardware considerations for different space modulation techniques, IEEE Trans. Wireless Commun. 16 (11) (2017) 7512–7522. http://dx.doi.org/10.1109/TWC.2017.2749399.

[10] R. Mesleh, S.S. Ikki, H.M. Aggoune, Quadrature spatial modulation, IEEE Trans. Veh. Technol. 64 (6) (2015) 2738–2742. http://dx.doi.org/10.1109/TVT.2014.2344036.

[11] R. Mesleh, S.S. Ikki, On the impact of imperfect channel knowledge on the performance of quadrature spatial modulation, in: Proc. Wireless Commun. Netw. Conf. WCNC, 2015, pp. 534–538. http://dx.doi.org/10.1109/WCNC.2015.7127526.

[12] M.M. Alwakeel, Quadrature spatial modulation performance analysis over Rician fading channels, J. Commun. 11 (3) (2016). http://dx.doi.org/10.12720/jcm.11.3.249-254.

[13] S. Koila, N. Neha, U. Sripati, Performance of Spatial-Modulation and spatial-multiplexing systems over Weibull fading channel, in: Proc. Int. Conf. Computing and Netw. Commun. CoCoNet, 2015, pp. 389–394. http://dx.doi.org/10.1109/CoCoNet.2015.7411215.

[14] A. Younis, R. Mesleh, H. Haas, Quadrature spatial modulation performance over Nakagami-m fading channels, IEEE Trans. Veh. Technol. 65 (12) (2016) 10227–10231. http://dx.doi.org/10.1109/TVT.2015.2478841.

[15] O.S. Badarneh, R. Mesleh, A comprehensive framework for quadrature spatial modulation in generalized fading scenarios, IEEE Trans. Commun. 64 (7) (2016) 2961–2970. http://dx.doi.org/10.1109/TCOMM.2016.2571285.

[16] L. Xiao, P. Yang, S. Fan, S. Li, L. Song, Y. Xiao, Low-complexity signal detection for large-scale quadrature spatial modulation systems, IEEE Commun. Lett. 20 (11) (2016) 2173–2176. http://dx.doi.org/10.1109/LCOMM.2016.2602210.

[17] Z. Yigit, E. Basar, Low-complexity detection of quadrature spatial modulation, IET Electron. Lett. 52 (20) (2016) 1729–1731. http://dx.doi.org/10.1049/el.2016.1583.

[18] I. Al-Nahhal, O. Dobre, S. Ikki, Quadrature spatial modulation decoding complexity: study and reduction, IEEE Wirel. Commun. Lett. 6 (3) (2017) 378–381. http://dx.doi.org/10.1109/LWC.2017.2694420.

[19] J. Li, X. Jiang, Y. Yan, W. Yu, S. Song, M.H. Lee, Low complexity detection for quadrature spatial modulation systems, Wirel. Pers. Commun. 95 (4) (2017) 4171–4183. http://dx.doi.org/10.1007/s11277-017-4057-y.

[20] B. Zheng, F. Chen, M. Wen, F. Ji, H. Yu, Y. Liu, Low-complexity ML detector and performance analysis for OFDM with in-phase/quadrature index modulation, IEEE Commu. Lett. 19 (11) (2015) 1893–1896. http://dx.doi.org/10.1109/LCOMM.2015.2474863.

[21] J. Li, M. Wen, X. Cheng, Y. Yan, S. Song, M.H. Lee, Generalized precoding-aided quadrature spatial modulation, IEEE Trans. Veh. Technol. 66 (2) (2017) 1881–1886. http://dx.doi.org/10.1109/TVT.2016.2565618.

[22] A. Afana, R. Mesleh, S. Ikki, I.E. Atawi, Performance of quadrature spatial modulation in amplify-and-forward cooperative relaying, IEEE Commun. Lett. 20 (2) (2016) 240–243. http://dx.doi.org/10.1109/LCOMM.2015.2509975.

[23] A. Afana, E. Erdogan, S. Ikki, Quadrature spatial modulation for cooperative MIMO 5G wireless networks, in: Proc. Globecom Workshops, GC Wkshps, 2016, pp. 1–5. http://dx.doi.org/10.1109/GLOCOMW.2016.7849011.

[24] A. Afana, I. Atawi, S. Ikki, R. Mesleh, Energy efficient quadrature spatial modulation MIMO cognitive radio systems with imperfect channel estimation, in: Proc. Ubiquitous Wireless Broadband (ICUWB) Conf. 2015, pp. 1–5. http://dx.doi.org/10.1109/ICUWB.2015.7324444.

[25] A. Afana, S. Ikki, R. Mesleh, I. Atawi, Spectral-efficient quadrature spatial modulation cooperative amplify and forward spectrum-sharing systems, IEEE Trans. Veh. Technol. 66 (3) (2017) 2857–2861. http://dx.doi.org/10.1109/TVT.2016.2580512.

[26] I.A. Mahady, A. Afana, R. Mesleh, S. Ikki, I. Atawi, Cognitive MIMO quadrature spatial modulation systems with mutual primary-secondary co-channel interference, in: Wireless Commun. Netw. Conf. WCNC, 2016, pp. 1–5. http://dx.doi.org/10.1109/WCNC.2016.7565136.

[27] Z. Yigit, E. Basar, Space-time quadrature spatial modulation, in: Proc. IEEE Int. Black Sea Conf. Commun. Netw. 2017. http://dx.doi.org/10.1109/BlackSeaCom.2017.8277677.

[28] R. Mesleh, A. Younis, Capacity analysis for LOS millimeter–wave quadrature spatial modulation, Wirel. Netw. (2017) 1–10. http://dx.doi.org/10.1007/s11276-017-1444-y.

[29] A. Younis, N. Abuzgaia, R. Mesleh, H. Haas, Quadrature spatial modulation for 5G outdoor millimeter-wave communications: capacity analysis, IEEE Trans. Wireless Commun. 16 (5) (2017) 2882–2890. http://dx.doi.org/10.1109/TWC.2017.2670545.

[30] E. Basar, U. Aygolu, E. Panayirci, H.V. Poor, Space-time block coded spatial modulation, IEEE Trans. Commun. 59 (3) (2011) 823–832. http://dx.doi.org/10.1109/TCOMM.2011.121410.100149.

[31] Polar coded spatial modulation, IET Commun. 8 (9) (2014) 1459–1466. http://dx.doi.org/10.1049/iet-com.2013.0499.
[32] E. Arikan, Channel polarization: A method for constructing capacity-achieving codes for symmetric binary-input memoryless channels, IEEE Trans. Inform. Theory 55 (7) (2009) 3051–3073. http://dx.doi.org/10.1109/TIT.2009.2021379.
[33] R. Mesleh, M. Di Renzo, H. Haas, P.M. Grant, Trellis coded spatial modulation, IEEE Trans. Wireless Commun. 9 (7) (2010) 2349–2361. http://dx.doi.org/10.1109/TWC.2010.07.091526.
[34] E. Basar, U. Aygolu, E. Panayirci, H.V. Poor, New trellis code design for spatial modulation, IEEE Trans. Wireless Commun. 10 (8) (2011) 2670–2680. http://dx.doi.org/10.1109/TWC.2011.061511.101745.
[35] G. Ungerboeck, Channel coding with multilevel/phase signals, IEEE Trans. Inform. Theory 28 (1) (1982) 55–67. http://dx.doi.org/10.1109/TIT.1982.1056454.
[36] C. Vladeanu, Turbo trellis-coded spatial modulation, in: Proc. IEEE Global Commun. Conf. GLOBECOM, 2012, pp. 4024–4029. http://dx.doi.org/10.1109/GLOCOM.2012.6503746.
[37] E. Basar, U. Aygolu, E. Panayirci, H.V. Poor, Super-orthogonal trellis-coded spatial modulation, IET Commun. 6 (17) (2012) 2922–2932. http://dx.doi.org/10.1049/iet-com.2012.0355.
[38] G. Yilmaz, E. Basar, U. Aygolu, Trellis coded space-shift keying modulation, in: Proc. IEEE 79th. Veh. Technol. Conf. VTC Spring, 2014, pp. 1–5. http://dx.doi.org/10.1109/VTCSpring.2014.7023131.
[39] M. Yacoub, G. Fraidenraich, J. Santos Filho, Nakagami-m phase-envelope joint distribution, Electron. Lett. 41 (5) (2005) 259–261. http://dx.doi.org/10.1049/el:20057014.
[40] M.K. Simon, M.-S. Alouini, Digital Communication Over Fading Channels, Wiley, 2005.
[41] G.L. Turin, The characteristic function of Hermitian quadratic forms in complex normal variables, Biometrika 47 (1/2) (1960) 199–201.
[42] D. Callan, When is rank additive?, College Math. J. 29 (2) (1998) 145–147.
[43] A. Paulraj, R. Nabar, D. Gore, Introduction to Space-time Wireless Communications, Cambridge University Press, 2003.

Zehra Yigit received her B.Sc. degree from University of Gaziantep, Gaziantep, Turkey, in 2013, and her M.Sc. Degree from Istanbul Technical University, Istanbul, Turkey, in 2017. Currently, she is a Ph.D. student and research assistant at Istanbul Technical University, Electronics and Communication Engineering Department. She has served as a reviewer for IET and IEEE journals. Her research interests include MIMO systems, spatial modulation, space–time coding and cooperative communications.

Ertugrul Basar was born in Istanbul, Turkey, in 1985. He received the B.S. degree (Hons.) from Istanbul University, Turkey, in 2007, and the M.S. and Ph.D. degrees from Istanbul Technical University, Turkey, in 2009 and 2013, respectively. From 2011 to 2012, he was with the Department of Electrical Engineering, Princeton University, Princeton, NJ, USA, as a Visiting Research Collaborator. He was an Assistant Professor with Istanbul Technical University from 2014 to 2017, where he is currently an Associate Professor of Electronics and Communication Engineering. He is an inventor of three pending/granted patents on index modulation schemes. His primary research interests include MIMO systems, index modulation, cooperative communications, OFDM, visible light communications, and signal processing for communications.

Recent recognition of his research includes the Young Scientists Award of the Science Academy (Turkey) in 2018, Turkish Academy of Sciences Outstanding Young Scientist Award in 2017, the first-ever IEEE Turkey Research Encouragement Award in 2017, and the Istanbul Technical University Best Ph.D. Thesis Award in 2014. He is also the recipient of four Best Paper Awards including one from the *IEEE International Conference on Communications 2016*. He has served as a TPC member for several IEEE conferences and is a regular reviewer for various IEEE journals. Dr. Basar currently serves as an Editor of the IEEE Transactions on Communications and *Physical Communication* (Elsevier), and as an Associate Editor of the IEEE Communications Letters.

Raed Mesleh has been with German Jordanian University, Amman, Jordan, since February 2016, where he is currently the vice dean of the school of electrical engineering and information technology, and an associate professor in the Department of Electrical and Communication Engineering. He received his Ph.D. in 2007 from Jacobs University in Bremen, Germany. From 2007 to 2010, he was a postdoctoral fellow at Jacobs University. He was with the Electrical Engineering Department at the University of Tabuk in Saudi Arabia from 2010–2015. During that period, he held the position of department chair and the director of research excellence and intellectual property units at the deanship of scientific research. He was a visiting scholar at Boston University, the University of Edinburgh, and Herriot–Watt University. His main research interests are in wireless communication and optical wireless communication with particular focus on MIMO techniques, mmWave communication,FSO and VLC. He is an inventor and co-inventor of eight patents. He invented a spatial modulation technique during his PhD, and he is the inventor of quadrature spatial modulation and trellis coded spatial modulation. He published more than 150 journal and conference papers with an overall citation of more than 5400. He received a distinguished researcher award at the University in Tabuk in 2013 and at German Jordanian University in 2016. In December 2016, he was awarded the Arab Scientific Creativity award from the Arab Thought Foundation.